ACS APPLIED MATERIALS & INTERFACES

Research Article

www.acsami.org

Flexible CuO Nanosheets/Reduced-Graphene Oxide Composite Paper: Binder-Free Anode for High-Performance Lithium-Ion Batteries

Yu Liu,[†] Wei Wang,[‡] Lin Gu,[‡] Yewu Wang,[‡] Yulong Ying,[†] Yiyin Mao,[†] Luwei Sun,[†] and Xinsheng Peng[†,§,*]

[†]State Key Laboratory of Silicon Materials, Department of Materials Science and Engineering [‡]Department of Physics & State Key Laboratory of Silicon Materials, and [§]Cyrus Tang Center for Sensor Materials and Applications, Zhejiang University, Hangzhou 310027, P. R. China

ABSTRACT: Flexible free-standing CuO nanosheets (NSs)/reduced graphene oxide (r-GO) hybrid lamellar paper was fabricated through vacuum filtration and hydrothermal reduction processes. A unique three-dimensional nanoporous network was achieved with CuO NSs homogeneously embedded within the r-GO layers. This hybrid lamellar composite paper was examined as a binder-free anode for lithium ion batteries, and demonstrated excellent cyclic retention with the specific capacity of 736.8 mA h g^{-1} after 50 cycles. This is much higher than 219.1 mA h g^{-1} of the pristine CuO NSs and 60.2 mA h g^{-1} of r-GO film at the same current density of 67 mA g^{-1}. The high capacitance and excellent cycling performance were generated from the integrated nanoporous structure compose of CuO NSs spaced r-GO layers, which offered an efficient electrically conducting channels, favored electrolyte penetration, and buffered to the volume variations during the lithiation and delithiation process. These outstanding electrochemical capabilities of CuO NSs/r-GO paper holds great promise for flexible binder-free anode for lithium ion batteries.

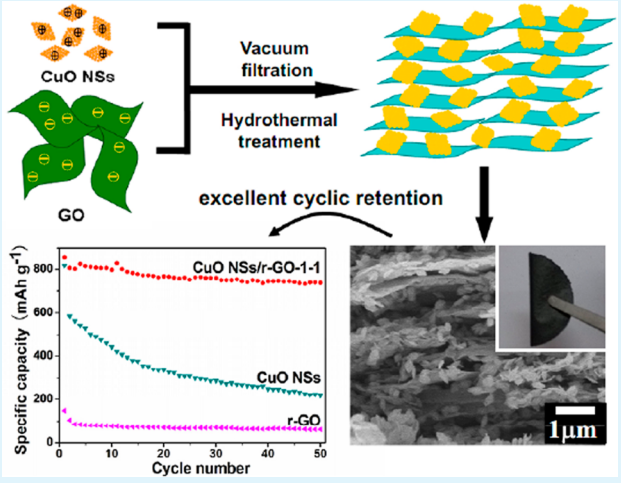

KEYWORDS: *flexible, CuO nanosheets/reduced-graphene oxide, binder-free anode, Li-ion battery*

1. INTRODUCTION

Because of the great demands for lithium-ion batteries (LIBs) and supercapacitor-based energy storage devices, tremendous effort has been paid to thin, flexible, and environmentally friendly energy storage devices.[1−3] Recently, high-performance flexible electrodes with excellent mechanical properties have drawn great attentions in portable electronics.[4,5] Besides conducting polymers, various carbon-based nanomaterials including carbon nanotubes, activated carbon, and carbon fibers are employed to construct thin and flexible electrodes.[6−11] Recently, graphene has been developed as a novel flexible electrodes in Li-ion batteries due to its unique structure, excellent mechanical properties and high electrical conductivity.[12−14] However, aggregation between reduced-graphene oxide (r-GO) sheets due to the strong van der Waals attraction can severely reduce the effective specific surface area and resulted a capacity of only 100 mA h g^{-1} as an anode in Li-ion batteries.[7,15] This is hard for high-performance energy storage devices.[7,15] To improve the capacity, researchers have explored various methods to construct paperlike flexible electrodes by introducing an electrochemically active component, which has higher capacity and stable cycle ability into the graphene.[16,17] These sandwiched structures can provide short transport length for both lithium ions and electrons because of the porous nature that accommodates volume change and favors electrolyte penetration. Besides, the nice electrical conductivity of graphene is beneficial to enhancing the capacitance and cycling performance.[18−20] Flexible SnO_2/r-GO nanocomposites paper,[14] MoO_3/r-GO hybrid films,[21] and TiO_2/r-GO hybrid paper[7] as LIBs anode materials have been reported.

CuO is low cost, nontoxic, and abundant and has high theoretical capacity (674 mA h g^{-1}), suggesting it is a promising anode alternative material for LIBs.[22,23] However, similar to the other transition metal oxide anodes, the poor electronic conductivity of CuO leads to the poor stability of repetitive cycling. Current studies have been mainly focused on increasing the electronic conductivity of the electrodes by adding conductive carbon materials.[24,25] Recently, our group reported CuO nanowire/CNT interpenetrating networks demonstrated a much higher electrochemical performance than that of pure

Received: July 31, 2013
Accepted: September 6, 2013
Published: September 6, 2013

   dx.doi.org/10.1021/am403136e | ACS Appl. Mater. Interfaces 2013, 5, 9850−9855

CuO nanowires for LIBs. The CNTs play dual functions in enhancing electronic conductivity and similar to elastic buffer absorbing stress induced by volume expansion.[26] Mai et al.[27] also found that CuO nanoparticles/r-GO composite showed better reversible capacity and cyclic performance than the CuO. They explained that the r-GO sheets constructed a conducting network for the fast electron transfer between the active materials and charge collector. In addition, the porous structure could serve as buffers to prevent the decomposition of the active materials due to the volume expansion/contraction during discharge/charge processes. However, binder-free CuO/r-GO paper anode for LIBs has been rarely reported. Here, we fabricated a flexible free-standing CuO NSs/r-GO nanoporous network paper by simple filtration combined with a hydrothermal reduction process. This flexible CuO NSs/r-GO paper were served as binder-free anode for LIBs with capacity of 736.8 mA h g^{-1}, which is 3.3 times higher than 219.1 mA h g^{-1} of pristine CuO NSs after 50 cycles at a rate of 67 mA h g^{-1}. This capacity is also much higher than the previous reported 576 mA h g^{-1} of CuO nanowire/CNT and 425.4 mA h g^{-1} for CuO nanoparticle/r-GO under similar test conditions.[26,27] The flexible free-standing CuO NSs/r-GO paper is expected in fabricating binder-free flexible anodes for LIBs.

2. EXPERIMENTAL SECTION

2.1. Materials. Copper nitrate ($Cu(NO_3)_2{\cdot}2.5H_2O$) and aminoethanol ($NH_2CH_2CH_2OH$) (AE) were received from Sigma-Aldrich without further purification before used. Graphite powder (99.95%) was obtained from Aladdin. Polycarbonate (PC) membrane (Whatman) with pore size of 200 nm, and effective diameters of 19 mm were used for the preparation of the composite paper by vacuum filtration. Millipore Direct-Q System produced 18.2 MΩ deionized water was used throughout the experiments.

2.2. Synthesis of CuO NSs and GO. The CuO NSs were synthesized by mixing a certain volume 2 mM $Cu(NO_3)_2$ aqueous solution with an equal volume of 1.6 mM AE aqueous solution with stirring for 1 min, then aging at a constant temperature of 25 °C for 24 h.[25,28] GO was prepared from graphite powder according to the modified Hummers' method.[29,30] Then GO was exfoliated in distilled water with a concentration of 0.2 mg/mL. The pH of the suspension was adjusted close to 6.2 using NaOH and HCl solutions.

2.3. Synthesis of CuO NSs/r-GO Papers. For a typical preparation of CuO NSs/r-GO composite, a certain amount of GO suspension was mixed with the prepared CuO NSs colloidal solution under vigorous stirring. Positively charged CuO NSs were quickly assembled with negatively charged GO sheets. A flocculent suspension was formed after a few minutes. Flexible CuO NSs/GO sandwich-like lamellar paper was fabricated by filtering the above flocculent suspension on a PC support using a SIBATA filtration system. After peeling from the PC, the obtained free-standing CuO NSs/GO paper was hydrothermal reduced by placing into a 50 mL Teflon-sealed autoclave with 30 mL of water and heated to 180 °C for 10 h.[27] After that, the paper was washed with ethanol and distilled water several times before drying at 60 °C for 4 h. In this work, three samples with mass ratios of CuO NSs to GO of 2:1, 1:1, and 1:2 were prepared, respectively, and named as CuO NSs/r-GO-2-1, CuO NSs/r-GO-1-1, and CuO NSs/r-GO-1-2. The detailed synthesis is schematically demonstrated in Scheme 1. The hydrothermal treated CuO NSs and r-GO were prepared following the same hydrothermal procedure as applied for CuO NSs/r-GO samples.

2.4. Electrode Preparation and Electrochemical Characterization. The free-standing electrodes were tested in coin-type cells to confirm the initial electrochemical performance. The as-prepared CuO NSs/r-GO paper (or r-GO paper) was directly used as working electrode without any binder and carbon black. Li metal foil was used as the negative electrode. The hydrothermal treated CuO NSs electrode was prepared by mixing the hydrothermal treated CuO NSs, carbon black, and polyvinylidene fluoride with a mass ratio of 8:1:1, and pasting onto pure copper foils, then pressed and dried under vacuum at 60 °C for 12 h. The coin cells were assembled in an argon-filled glovebox. The electrolyte was a 50:50 (w/w) ethylene carbonate and diethyl carbonate mixture solution with 1 M $LiPF_6$. The galvanostatic charge−discharge performances of the cells were tested in the voltage range of 0.01−3.0 V under a constant current density of 67 mA g^{-1} (0.1C) by EQ-BST8-WA battery-test system. Cyclic voltammetry (CV) was recorded by a CHI 660D (Chenhua Shanghai, China) electrochemical workstation in the voltage range 0.01−3.0 V with a scan rate of 0.1 mV s^{-1}. Electrochemical impedance spectroscopy (EIS) results were obtained from a frequency range of 100 kHz to 1 Hz.

Scheme 1. Schematic of the Synthesis Procedure of CuO NSs/r-GO Paper

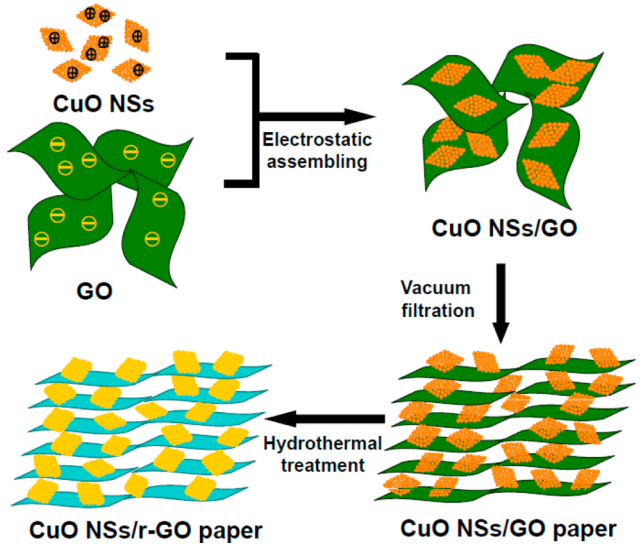

2.5. Characterization. Crystal structure information is obtained by X-ray diffraction (XRD) at room temperature using an X'Pert PRO (PANalytical, Netherlands) instrument with Cu *Kα* radiation. Scanning electronic microscopy (SEM) (Hitachi S-4800), transmission electron microscopy (TEM, Philips CM200) were used to characterize the morphologies. Further evidence for the composition of the product was recorded from X-ray photoelectron spectroscopy (XPS), using an ESCALAB_250Xi X-ray photoelectron spectrometer with Al *Kα* X-ray as the excitation source. Raman spectra were conducted on the Renishaw inVia Raman microscope under the excitation length of 532 nm. The specific surface area was calculated by Brunauer−Emmett−Teller (BET) method using a Quantachrome Autosorb-1 apparatus.

3. RESULTS AND DISCUSSION

the XRD patterns of the as-prepared CuO NSs/GO and CuO NSs/r-GO papers are presented in Figure 1a, respectively. The patterns obviously consist of two sets of diffraction peaks, all the asterisk marked peaks match very well with standard CuO phase (JCPDS standard card no.45−0937). The diffraction peak at 9.03° of CuO NSs/GO is a typical peak of GO paper with the interlayer distance of ∼0.98 nm.[30] For CuO NSs/r-GO, the broadened peak (002) at 23.4°, indicates the successful reduction of GO and good interaction between the r-GO layers. Figure 1b shows XPS spectra of CuO NSs/r-GO paper. In the survey region (0−1200 eV), it is clear that C, O, and Cu elements coexist in the sample. Figure 1c is the high-resolution spectrum of Cu. The peaks observed at 933.9 and 953.6 eV are assigned to $Cu2p_{3/2}$ and $Cu2p_{1/2}$, which are higher than the peak positions for Cu (0) metal and are attributed to oxidized

dx.doi.org/10.1021/am403136e | ACS Appl. Mater. Interfaces 2013, 5, 9850−9855

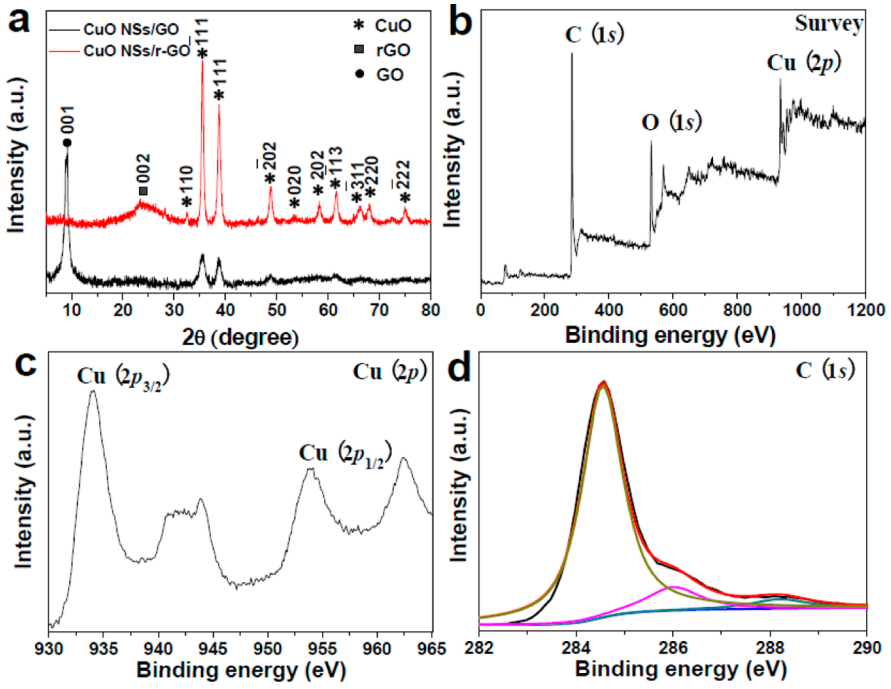

Figure 1. (a) XRD patterns of CuO NSs/GO and CuO NSs/r-GO paper. XPS spectra of (b) the survey scan, (c) Cu 2p, and (d) C 1s region of the CuO NSs/r-GO paper.

Cu(II).[31] Additionally, two satellite peaks at 943.8 and 962.4 eV, further confirm that the oxide in the sample are CuO. Figure 1d displays a high-resolution spectrum of C, it can be fitted into three peaks at 284.5, 285.8, and 288.2 eV, which are referred to C−C, C−O, and C═O vibrations, respectively.[32−34] It is obviously seen that the peak intensity of C−O and C═O is much weaker than that of C−C, which indicates that most of the oxygen-containing groups are removed after hydrothermal treatment.[32,35]

Figure 2 shows the Raman spectra of the as-prepared CuO NSs/GO-1-1 and CuO NSs/r-GO-1-1. The characteristic D

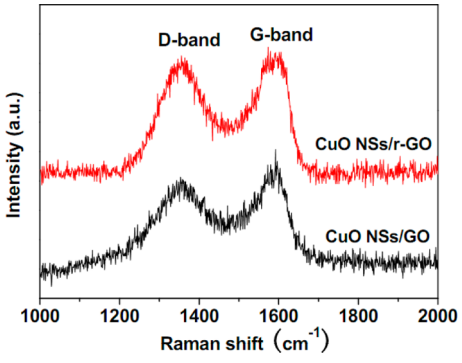

Figure 2. Raman spectra of CuO NSs/GO1-1 and CuO NSs/r-GO-1-1 papers.

and G bands of graphene based materials were observed from these two composites.[11] In general, the I_D/I_G reflects the defect density in graphene planes. After hydrothermal treatment, the ratio of the intensity of D to G band (I_D/I_G) increases from 1.12 to 1.26, suggesting that the reduction of exfoliated GO introduces more defects into the CuO NSs/r-GO samples.[11]

Images a and b in Figure 3 display the top-view SEM images of CuO NSs/GO and CuO NSs/r-GO paper, respectively. It is

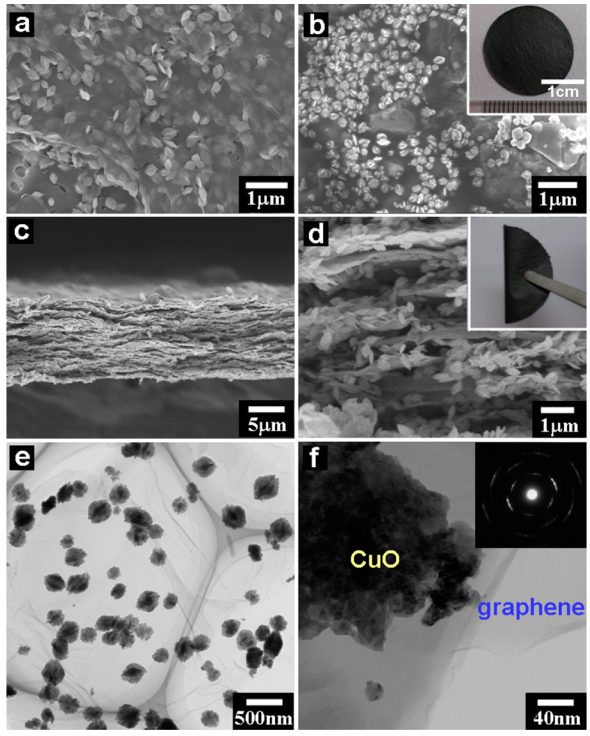

Figure 3. (a, b) Top-view SEM images of the CuO NSs/GO and CuO NSs/r-GO paper, the inset in b is a digital photograph of CuO NSs/r-GO paper with diameter of ca. 19 mm. (c, d) Cross-section SEM images of the CuO NSs/r-GO paper, which shows good flexibility (the inset in d). (e, f) TEM images of the CuO NSs/r-GO paper, inset of (f) is electron diffraction pattern.

clearly observed that the well-dispersed CuO NSs are anchored onto the both sides of GO and r-GO sheets. The CuO nanosheets are in size of 300 nm. The inset in Figure 3b shows CuO NSs/r-GO paper with diameter of ca. 19 mm. From the

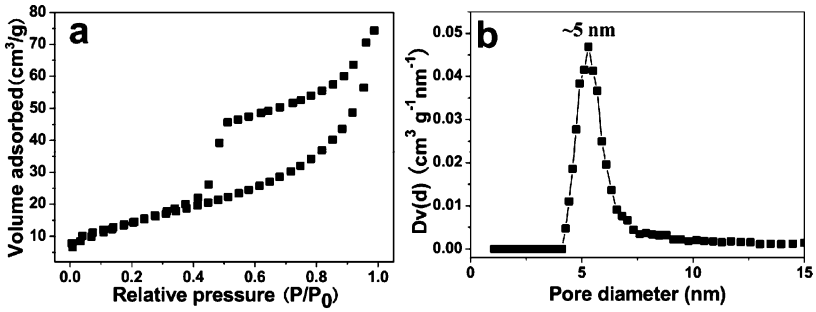

Figure 4. (a) Nitrogen adsorption and desorption isotherms of CuO NSs/r-GO paper and (b) the corresponding pore size distribution plots.

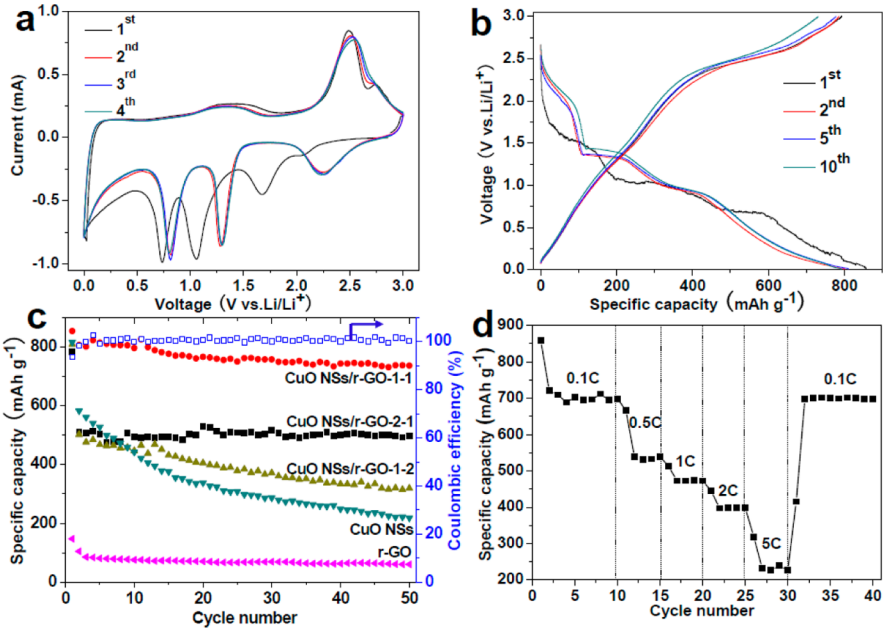

Figure 5. (a) CV curves of CuO NSs/r-GO at a scan rate of 0.1 mV s^{-1}. (b) Charge−discharge curves of the CuO NSs/r-GO-1-1 paper. (c) Cycling performance of r-GO, CuO, CuO NSs/r-GO-2-1, CuO NSs/rGO-1-1, and CuO NSs/r-GO-1-2 at constant current density of 67 mA g^{-1}. (d) Cycling performance of CuO NSs/r-GO-1-1 at different rates from 0.1 to 5 *C*.

cross-sectional view, (Figure 3c, d) in the hybrid CuO NSs/r-GO paper, CuO NSs are uniformly incorporated between the r-GO layers, resulting in sandwiched structures. The inset in Figure 3d shows that the CuO NSs/r-GO paper has good flexibility. The r-GO layers formed a 3D continuous network, which function as both a mechanical support and current collector. Simultaneously, CuO NSs expanded the interlayer spacing between the r-GO layers and prevented their agglomeration, which can greatly facilitate electrolyte diffusion compared with the compactly packed structure. Here, many additional pores are constructed between the CuO NSs and r-GO layers, which will facilitate ion diffusivity and provide large reaction sites on the surface, and is therefore favorable for the electrochemical process. Figure 3e shows the low-magnification TEM image of CuO NSs/r-GO composites. CuO NSs are uniformly distributed on the surface of r-GO sheets. Some wrinkles and folds are found in rGO sheets (black area in Figure 3e), which is typical for rGO sheets.[29] The high-magnification TEM image further confirms the good connection of CuO NSs and r-GO. Several concentric diffraction rings in selected area electron diffraction pattern (inset of Figure 3f) recorded on the CuO nanosheets indicate the CuO nanosheets are polycrystalline.

The N_2 gas adsorption−desorption isotherms of CuO NSs/r-GO-1−1 is shown in Figure 4. The BET surface area of it is 53.2 m^2 g^{-1}, and much higher than 14.9 m^2 g^{-1} of r-GO and 29.5 m^2 g^{-1} of the hydrothermal treated CuO NSs.[35] In addition, the average pore diameter is found nearly 5 nm by the pore-size distribution analysis (Figure 4b).

The CV curves of CuO NSs/r-GO composite at a scan rate of 0.1 mV/s is shown in Figure 5a. Three reduction peaks are observed at 0.73 V, 1.05 and 1.65 V (vs Li^+/Li) during the first discharge cycle. These peaks indicate a multistep electrochemical process, including the formation of solid solid-solution phase with a CuO-type structure, then converting into a Cu_2O phase, and further to Cu; the formation of Li_2O; and a solid electrolyte interphase (SEI) layer generating on the electrode surface.[23,36−38] During the subsequent charging process, three anodic peaks located at 1.42, 2.48, and 2.75 V are observed, which corresponds to the decomposition of the organic layer and the partial oxidization of copper to the Cu(I) and Cu(II), respectively.[27,36] The electrochemical reaction mechanism can be described as[23]

$$CuO + 2Li^+ + 2e^- \Leftrightarrow Cu + Li_2O$$

The subsequent CV curves (2nd, third and fourth) demonstrate that the redox reaction is well reversible. Figure

dx.doi.org/10.1021/am403136e | ACS Appl. Mater. Interfaces 2013, 5, 9850−9855

5b shows the first, second, fifth and 10th charge/discharge voltage profiles of the CuO NSs/r-GO nanocomposites paper at a rate of 0.1 *C* (*C* = 670 mA g^{-1}). In the first cycle, the constant slope with several small plateaus indicates a multiphase transition between CuO and lithium. The initial discharge and charge capacities are found to be 854.3 and 782.3 mA h g^{-1}, respectively. The irreversible capacity loss may result from the diverse irreversible processes, such as interfacial lithium storage, the formation of SEI layer and organic conductive polymer, as well as the electrolyte decomposition.[36−38]

To optimize the properties of LIBs, we examined three kinds of mass ratios of CuO NSs to r-GO, including 2:1, 1:1, and 1:2. The cycling performance profiles at a rate of 0.1 C are exhibited in Figure 5c. All of these three components showed the high initial discharge specific capacity, which are higher than the theoretical specific capacity of 674 mA h g^{-1} based on a maximum uptake of two Li^+ per CuO. This phenomenon was usually contributed to the formation of a SEI layer, the reduction of adsorbed impurities on surface of component and so on. However, the pure CuO nanosheets anode exhibited a low discharge specific capacity of 219.1 mA h g^{-1} after 50 cycles at a rate of 0.1 C. The above results indicate that the introduction of r-GO into CuO NSs significantly enhances the cyclic performance and capacity. Among the three CuO NSs/r-GO samples with different CuO to r-GO ratios, CuO NSs/r-GO with mass ratio of 1:1 has the highest retaining discharge specific capacity of 736.8 mA h g^{-1}, which is about 3.3 times higher than that of CuO NSs. This performance is remarkable compared with the best values reported previously (see Table 1).[23−27,36] Considering the electrochemical capacity of r-GO,

Table 1. Comparison of Various CuO/Carbon Materials for LIBs

materials	current density (mA g^{-1})	cycle number	specific capacity (mA h g^{-1})
CuO nanoparticles/r-GO	67	50	425.4[27]
CuO nanoparticles/r-GO	50	50	743[24]
CuO nanoparticles/r-GO	120	30	500[36]
CuO NSs/CNT	67	40	571[25]
CuO nanowire/CNT	67	50	576[26]
CuO nanospheres/CNT	160	50	500[23]
free-standing CuO NSs/r-GO	67	50	736.8 (this work)

the cycling performance of r-GO paper as anode was also tested. The discharge specific capacity stably kept at 60.2 mA h g^{-1} after 50 cycles. It proves that the discharge specific capacity retention of CuO NSs/r-GO is mainly contributed by the CuO NSs. The r-GO plays a significant role in improving the cyclic stability, due to the excellent electric conductivity and the firm 3D-networks of the r-GO porous structures in the CuO NSs/r-GO paper. The Coulombic efficiency of CuO NSs/r-GO-1-1 is shown in Figure 5c. The Coulombic efficiency of the composite paper at the 67 mA g^{-1} current rates is nearly 100% from the third cycle to subsequent cycles. Furthermore, we investigated the relation of different discharge rates with specific capacity for CuO NSs/r-GO-1-1 from 0.1 to 5 *C* and the results are shown in Figure 5d. After 10 cycles at a rate of 0.1 *C*, the discharge specific capacity is still maintained at 697.8 mA g^{-1}.This value decreases with increasing discharge rate. However, when the discharge rate recovers to 0.1 C, the discharge specific capacity still exceeds 698.0 mA g^{-1}. The excellent reversibility reflects its preeminent stability during electrochemical reaction. And this also proves that introducing r-GO into CuO NSs to form sandwiched networks can remarkably increases its electrochemical performance. One possible reason for the capacity of CuO NSs/r-GO-1-1 sample higher than the theoretical values might be due to the formation of gel-like polymer layer on the surface of the CuO NSs by electrolyte decomposition as demonstrated in Co_3O_4 nanostructured anodes.[39] This gel-like polymer surface layer possibly would contribute to the additional lithium storage on its surface in a capacitive way, and resulting in the observed extra capacity. The incorporation of r-GO not only increased the surface area of the active materials but also prevented the decomposition of CuO NSs during the lithination and delithination process. Then the contribution coming from the gel-like surface layer is significant and observable in CuONSs/r-GO-1-1.

Electrochemical impedance spectroscopy (EIS) measurements were employed to deeply understand the electrochemical performance of the CuO NSs/r-GO paper and the hydrothermal treated pure CuO NSs,. The EIS spectra are equivalent to a circuit. As shown in inset of Figure 6, *R* in the high

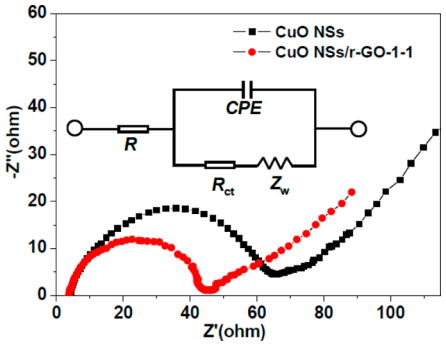

Figure 6. Nyquist plots of CuO NSs/r-GO-1-1 paper and hydrothermal treated CuO NSs. The inset presents the equivalent circuit model.

frequency region is related to the ohmic resistance and R_{ct} is the charge-transfer resistance, respectively. The constant phase element (CPE) account for the double layer capacitance, and Z_W at low frequencies represents the Warburg impedance related to lithium ion diffusion.[23,40] The typical characteristics of the two Nyquist plots are observed with one semicircle in the high-medium frequency range and a sloping straight line in the low-frequency range. The spectra appeared in the medium frequency range is classically assigned to the charge-transfer resistance occurring between active materials and liquid electrolyte. The straight line is attributed to the lithium-diffusion process within electrodes.[12,41] It clearly shows the diameter of the semicircle for the CuO NSs/r-GO electrode is much smaller than that of the pure CuO nanosheets electrode, because the CuO NSs/r-GO has lower electron-transfer resistance. This implies that the r-GO make charge transfer much easily at the electrode/electrolyte interface, and consequently decrease the internal resistance.

4. CONCLUSION

In summary, a free-standing flexible CuO NSs/r-GO paper has been prepared by a vacuum filtration method and hydrothermal

reduction process. This paper could be used as binder-free anode for LIBs. The highly conductive r-GO functioned as both a mechanical support and an embedded current collector. The unique sandwiched structure of r-GO and CuO NSs composite paper resulted in fast Li ion diffusion and excellent rate performance and cyclic stability. Accordingly, this design provides a promising candidate for binder-free flexible anode for lithium-ion batteries.

AUTHOR INFORMATION

Corresponding Author

*E-mail: pengxinsheng@zju.edu.cn. Fax: 86-571-87952625. Tel: 86-571-87951958.

Notes

The authors declare no competing financial interest.

ACKNOWLEDGMENTS

This work was supported by the National Natural Science Foundations of China (NSFC 21003105, 21271154, 51272232), Doctoral Fund of Ministry of Education of China (20110101110028), and the project-sponsored by SRF for ROCS, SEM.

REFERENCES

(1) Yuan, L. Y.; Lu, X. H.; Xiao, X.; Zhai, T.; Dai, J. J.; Zhang, F. C.; Hu, B.; Wang, X.; Gong, L.; Chen, J.; Hu, C. G.; Tong, Y. X.; Zhou, J.; Wang, Z. L. *ACS Nano* **2012**, *6*, 656−661.
(2) Goyal, A.; Reddy, A. L. M.; Ajayan, P. M. *Small* **2011**, *7*, 1709−1713.
(3) Li, Z. Q.; Liu, N. N.; Wang, X. K.; Wang, C. B.; Qi, Y. X.; Yin, L. W. *J. Mater. Chem.* **2012**, *22*, 16640−16648.
(4) Gao, H. C.; Xiao, F.; Ching, C. B.; Duan, H. W. *ACS Appl. Mater. Interfaces* **2012**, *4*, 7020−7026.
(5) Zhao, B.; Shao, Z. P. *J. Phys. Chem. C* **2012**, *116*, 17440−17447.
(6) Zhang, K.; Zhang, L. L.; Zhao, X. S.; Wu, J. S. *Chem. Mater.* **2010**, *22*, 1392−1401.
(7) Hu, T.; Sun, X.; Sun, H. T.; Yu, M. P.; Lu, F. Y.; Liu, C. S.; Lian, J. *Carbon* **2013**, *51*, 322−326.
(8) Noerochim, L.; Wang, J. Z.; Chou, S. L.; Wexler, D.; Liu, H. K. *Carbon* **2012**, *50*, 1289−1297.
(9) Etacheri, V.; Sharon, D.; Garsuch, A.; Afri, M.; Frimerand, A. A.; Aurbach, D. *J. Mater. Chem. A* **2013**, *1*, 5021−5030.
(10) Lang, L. M.; Xu, Z. *ACS Appl. Mater. Interfaces* **2013**, *5*, 1698−1703.
(11) Huang, G. C.; Chen, T.; Wang, Z.; Chang, K.; Chen, W. X. *J. Power Sources* **2013**, *235*, 122−128.
(12) Wang, R. H.; Xu, C. H.; Sun, J.; Gao, L.; Lin, C. C. *J. Mater. Chem. A* **2013**, *1*, 1794−1800.
(13) Chen, Y.; Song, B. H.; Lu, L.; Xue, J. M. *Nanoscale* **2013**, *5*, 6797−6803.
(14) Prabakar, S. J. R.; Hwang, Y. H.; Bae, E. G.; Shim, S.; Kim, D.; LA h, M. S.; Sohn, K. S.; Pyo, M. *Adv. Mater.* **2013**, *25*, 3307−3312.
(15) Wang, C. Y.; Li, D.; Too, C. O.; Wallace, G. G. *Chem. Mater.* **2009**, *21*, 2604−2606.
(16) Zhou, J. G.; Wang, J.; Zuin, L.; Regier, T.; Hu, Y. F.; Wang, H. L.; Liang, Y. Y.; Maley, J.; Sammynaikenc, R.; Dai, H. J. *Phys. Chem. Chem. Phys.* **2012**, *14*, 9578−9581.
(17) Byon, H. R.; Gallant, B. M.; Lee, S. W.; Shao-Horn, Y. *Adv. Funct. Mater.* **2013**, *23*, 1037−1045.
(18) Wang, D. H.; Kou, R.; Choi, D.; Yang, Z. G.; Nie, Z. M.; Li, J.; Saraf, L. V.; Hu, D. H.; Zhang, J. G.; Graff, G. L.; Liu, J.; Pope, M. A.; Aksay, I. A. *ACS Nano* **2010**, *4*, 1587−1595.
(19) Wang, R. H.; Xu, C. H.; Sun, J.; Liu, Y. Q.; Gao, L.; Lin, C. C. *Nanoscale* **2013**, *5*, 6960−6967.
(20) Zhou, X. S.; Cao, A. M.; Wan, L. J.; Guo, Y. G. *Nano Res.* **2012**, *5*, 845−853.
(21) Noerochim, L.; Wang, J. Z.; Wexler, D.; Chao, Z.; Liu, H. K. *J. Power Sources* **2013**, *228*, 198−205.
(22) Chen, H.; Feng, F.; Hu, Z. L.; Liu, F. S.; Gong, W. Q.; Xiang, K. X. *Trans. Nonferrous Met. Soc. China* **2012**, *22*, 2523−2528.
(23) Zhang, Y.; Xu, M. W.; Wang, F.; Song, X. P.; Wang, Y. H.; Yang, S. *J. Phys. Chem. C* **2013**, *117*, 12346−12351.
(24) Zhou, J. S.; Ma, L. L.; Song, H. H.; Wu, B.; Chen, X. H. *Electrochem. Commun.* **2011**, *13*, 1357−1360.
(25) Huang, H. W.; Liu, Y.; Wang, J. H.; Gao, M. X.; Peng, X. S.; Ye, Z. Z. *Nanoscale* **2012**, *5*, 1785−1787.
(26) Huang, H. W.; Yu, Q.; Ye, Y. H.; Wang, P.; Zhang, L. Q.; Gao, M. X.; Peng, X. S.; Ye, Z. Z. *CrystEngComm* **2012**, *14*, 7294−7300.
(27) Mai, Y. J.; Wang, X. L.; Xiang, J. Y.; Qiao, Y. Q.; Zhang, D.; Gu, C. D.; Tu, J. P. *Electrochim. Acta* **2011**, *56*, 2306−2311.
(28) Liu, Y.; Huang, H. W.; Peng, X. S. *Electrochim. Acta* **2013**, *104*, 289−294.
(29) Liu, Y.; Hu, Y.; Zhou, M. J.; Qian, H. S.; Hu, X. *Appl. Catal., B* **2012**, *125*, 425−431.
(30) Huang, H. B.; Mao, Y. Y.; Ying, Y. L.; Liu, Y.; Sun, L. W.; Peng, X. S. *Chem. Commun.* **2013**, *49*, 5963−5965.
(31) Durando, M.; Morrish, R.; Muscat, A. J. *J. Am. Chem. Soc.* **2008**, *130*, 16659−16668.
(32) Liu, S.; Tian, J. Q.; Wang, L.; Luo, Y. L.; Sun, X. P. *Catal. Sci. Technol.* **2012**, *2*, 339−344.
(33) Liu, J. B.; Fu, S. H.; Yuan, B.; Li, Y. L.; Deng, Z. X. *J. Am. Chem. Soc.* **2010**, *132*, 7279−7281.
(34) Lee, J. W.; Hall, A. S.; Kim, J. D.; Mallouk, T. E. *Chem. Mater.* **2012**, *24*, 1158−1164.
(35) Liu, Y.; Ying, Y. L.; Mao, Y. Y.; Gu, L.; Wang, Y. W.; Peng, X. S. *Nanoscale* **2013**, *5*, 9134−9140.
(36) Seo, S. D.; Lee, D. H.; Kim, J. C.; Lee, G. H.; Kim, D. W. *Ceram. Int.* **2013**, *39*, 1749−1755.
(37) Xiang, J. Y.; Tu, J. P.; Qiao, Y. Q.; Wang, X. L.; Zhong, J.; Zhang, D.; Gu, C. D. *J. Phys. Chem. C* **2011**, *115*, 2505−2513.
(38) Xu, M. W.; Wang, F.; Ding, B. J.; Song, X. P.; Fang, J. X. *RSC Adv.* **2012**, *2*, 2240−2243.
(39) Li, L.; Seng, K. H.; Chen, Z. X.; Guo, Z. P.; Liua, H. K. *Nanoscale* **2013**, *5*, 1922−1928.
(40) Rahman, M. M.; Wang, J. Z.; Hassan, M. F.; Wexler, D.; Liu, H. K. *Adv. Energy Mater.* **2011**, *1*, 212.
(41) Liang, J. F.; Zhao, Y.; Guo, L.; Li, L. D. *ACS Appl. Mater. Interfaces* **2012**, *4*, 5742−5748.